Control of Active Component of Current in Dual Active Bridge Converter

Suyash Sushilkumar Shah* and Subhashish Bhattacharya†
Department of Electrical and Computer Engineering
North Carolina State University, Raleigh, NC 27695, USA
Email: *sshah7@ncsu.edu, †sbhatta4@ncsu.edu

***Abstract*—The paper presents a control strategy based on improved first harmonic approximation model of the single-phase dual active bridge (DAB) converter. The model consists of three state-variables: output DC voltage and two orthogonal components of first harmonic of transformer current, equivalent to active and circulating powers. Foremost, a strategy based on the conventional output voltage control is designed to regulate the output voltage. Subsequently, the *first harmonic current control* strategy, which aims to control the active power component of the current to regulate the output DC voltage, is introduced. Based on this strategy, a method to design the control system is suggested and its implementation in digital domain is described. The two control strategies are validated through time-domain simulations. Finally, the schemes are implemented for a prototype 500V/270V DC/DC converter. The experimental results are reported and compared against the developed control models for verification.**

***Keywords*—Bidirectional dc-dc converter, current control, DAB control, dual active bridge, first harmonic approximation.**

NOMENCLATURE

n	Turns-ratio of the transformer
ω	Switching frequency (rad/s)
T_s	Switching cycle period (s)
ϕ	Phase-shift between converter-bridge voltages
L	Power transfer and leakage inductance (H)
C	DC-side output capacitance (F)
R	Load resistance (Ω)
v_{in}	Input voltage (V)
v_C	Output capacitor voltage (V)
i_L	Secondary side transformer current (A)
$\Im\langle i_L\rangle_1$	Active power component of inductor current
$\Re\langle i_L\rangle_1$	Circulating power component of inductor current
γ	Correction factor
$G_{v_c\phi}$	Plant for output voltage to phase-shift angle, ϕ
$G_{v_c,\Im\langle i_L\rangle_1}$	Plant for output voltage to $\Im\langle i_L\rangle_1$
$G_{\Im\langle i_L\rangle_1,\phi}$	Plant for $\Im\langle i_L\rangle_1$ to phase-shift angle, ϕ

I. INTRODUCTION

The dual active bridge (DAB) converter, shown in Fig. 1, was introduced by De Doncker, *et al.* [1] in 1991. It is popular for bidirectional power conversion in applications ranging from solid-state transformers [2] to automotives [3]. Several modeling and current control techniques have been developed for the DAB converter [1], [4]–[10]. Most methods for current control of DAB converter are based on instantaneous peak or valley current [8], [9]. Han, *et al.* [8] utilize slope compensation in a manner similar to

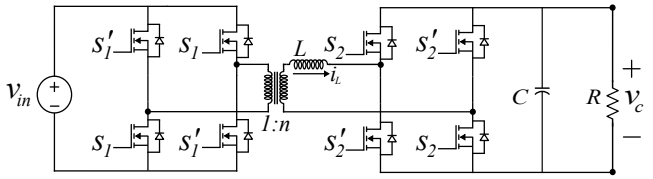

Fig. 1: Circuit topology of a single-phase DAB converter.

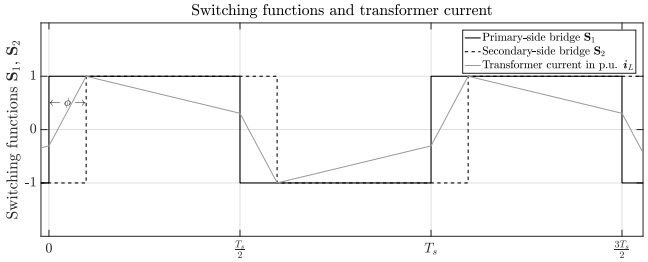

Fig. 2: Representative switching functions and transformer current in phase-shift modulated DAB converter.

that applied to non-isolated DC/DC converters. Variations of peak current control, such as predictive current control [10] and hysteresis current control [11] are also reported. These strategies, however, do not allow control of active power component of current in the DAB converter.

In this paper, improved first harmonic approximation (I-FHA) model [4] has been utilized to propose a *first harmonic current control* strategy. The I-FHA models the DAB converter as two fundamental frequency AC voltage sources connected through a power transfer inductance L, shown in Fig. 3a. The secondary side AC voltage lags the primary side by a phase-shift angle, ϕ (Fig. 2). The I-FHA model uses Fourier series expansion of AC quantities. It allows decomposition of fundamental frequency component of transformer/inductor current into two parts, as shown in Fig. 3b. The imaginary part, $\Im\langle i_L\rangle_1$, in phase with the primary side AC voltage, is the active power component; the real part, $\Re\langle i_L\rangle_1$, in quadrature, is the circulating power component. Such a model and the derived control strategy can independently control the active power component of the current. In the proposed strategy, the phase-shift angle (ϕ) is controlled to regulate the active power component of first harmonic transformer current, $\Im\langle i_L\rangle_1$; which, in turn regulates the output DC voltage.

The paper also discusses the susceptibility of DAB

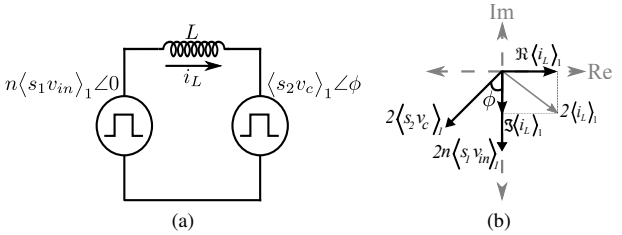

Fig. 3: Modeling of DAB converter: (a) Equivalent model and (b) representative phasor diagram of first harmonic AC voltages and currents of DAB converter.

converter to transient DC component in transformer current when a step-change in reference voltage is applied. Several authors have tackled the issue through a version of one of the following methods: (a) peak or peak-valley current control [8]–[10], (b) compensation by varying the rising and/or falling edges of one of the bridge voltages [12]–[14], (c) filtering the DC component of the high frequency AC current or flux and compensating using the duty-ratio of the bridge voltages [15]–[17]. The proposed control, inherently, mitigates the transient DC, thereby reducing the peak flux density, B_m, in the inductor and the peak semiconductor current, in comparison to the conventional *output voltage control* strategy. The effectiveness of *first harmonic current control* is demonstrated through time-domain simulations by comparing it against the conventional *output voltage control* of a 3 kW, 500V/270V prototype system.

In this paper, the I-FHA model is used to design two control strategies: conventional *output voltage control* and *first harmonic current control*. The paper is organized as follows: section II briefly introduces the concept of Fourier series expansion of AC quantities to generate a generalized average model. The I-FHA model of the DAB converter is introduced, thereafter. A system based on *output voltage control* strategy is designed for given system parameters in section III. Subsequently, in section IV, *first harmonic current control* strategy is proposed. A method to design the inner current control loop and outer voltage control loop is outlined. Further, a scheme to implement the proposed control in a digital signal processor is explored. The time-domain results for both control strategies are presented in section V, along with their experimental verification. The capability of *first harmonic current control* to mitigate the DC transient appearing in the inductor current is discussed and compared against that of the *output voltage control* through time-domain simulations. The conclusions are summarized in section VI.

II. Improved First Harmonic Approximation

In this section, the use of Fourier series expansion and its complex and trigonometric coefficients in generalized average modeling technique [18] is recounted. The improved first harmonic approximation (I-FHA) model [4], based on generalized average modeling technique, is briefly introduced.

A. Generalized average model

The generalized average modeling (GAM) uses Fourier series expansion (1) to represent the inductor currents and capacitor voltages in the power converters [18]. Any periodic waveform can be expanded to its Fourier representation in complex coefficient or trigonometric terms. The complex Fourier coefficients of any electrical quantity, x, are $\langle x\rangle_k$ and $\langle x\rangle_{-k}$. These are related to the trigonometric terms, $\Re\langle x\rangle_k$ and $\Im\langle x\rangle_k$ respectively, through (2). $\Re\langle x\rangle_k$ is the k^{th} coefficient in Fourier cosine series of x and $\Im\langle x\rangle_k$ is the k^{th} coefficient in Fourier sine series of x.

$$\langle x\rangle_k = \frac{1}{T}\int_0^T x(\tau)\, e^{-jk\omega\tau} d\tau \tag{1}$$

$$\langle x\rangle_k = \langle x\rangle^*_{-k} = \frac{1}{2}\Big(\Re\langle x\rangle_k + j\cdot\Im\langle x\rangle_k\Big) \tag{2}$$

B. Large-signal model based on improved-FHA method

The model of the DAB converter, as reported in [4], is described in (3). The correction factor, γ, allows for inclusion of the active power transmitted through harmonic voltages and currents without the associated complexity. The model comprises of three state-variables representing the output capacitor voltage, $\langle v_C\rangle_0$, and orthogonal components, $\Re\langle i_L\rangle_1$ and $\Im\langle i_L\rangle_1$ of the inductor current. $\Re\langle i_L\rangle_1$ represents the circulating power component and $\Im\langle i_L\rangle_1$ represents the active power component of the current.

$$\begin{aligned}
\frac{d}{dt}\Re\langle i_L\rangle_1 &= \frac{1}{L}\frac{4}{\pi}\sin\phi\langle v_C\rangle_0 + \omega\Im\langle i_L\rangle_1 \\
&\quad + (\gamma-1)\frac{4}{\pi}\frac{n}{\omega L}\frac{d}{dt}\langle v_{in}\rangle_0 \\
\frac{d}{dt}\Im\langle i_L\rangle_1 &= \frac{1}{L}\left[-n\cdot\frac{4}{\pi}\langle v_{in}\rangle_0 + \frac{4}{\pi}\cos\phi\langle v_C\rangle_0\right] - \omega\Re\langle i_L\rangle_1 \\
\frac{d}{dt}\langle v_C\rangle_0 &= \frac{1}{C}\left[-\frac{4}{2\pi}\sin\phi\Big(\Re\langle i_L\rangle_1\Big) - \frac{4}{2\pi}\cos\phi\Big(\Im\langle i_L\rangle_1\Big)\right] \\
&\quad - \frac{1}{(R\gamma)C}\langle v_C\rangle_0
\end{aligned} \tag{3}$$

The large signal model (4) is extracted by setting the time-derivative terms in the full model (3) to zero. The I-FHA method modifies the load resistance R to an equivalent load of $R\gamma$, compensating for the unaccounted harmonic power.

$$\begin{bmatrix} 0 & \omega & \frac{4}{\pi}\frac{\sin\phi}{L} \\ -\omega & 0 & \frac{4}{\pi}\frac{\cos\phi}{L} \\ -\frac{4}{2\pi}\frac{\sin\phi}{C} & -\frac{4}{2\pi}\frac{\cos\phi}{C} & -\frac{1}{(R\gamma)C} \end{bmatrix} x = -\begin{bmatrix} 0 \\ -\frac{n}{L}\frac{4}{\pi} \\ 0 \end{bmatrix}\langle v_{in}\rangle_0$$
$$\text{where, } x = \begin{bmatrix}\Re\langle i_L\rangle_1 & \Im\langle i_L\rangle_1 & \langle v_C\rangle_0\end{bmatrix}^T \tag{4}$$

III. Output voltage control

In this section, the *output voltage control* is designed for DAB converter system with parameters listed in Table I. The structure of the conventional *output voltage control* system is shown in Fig. 4a. Here, the output voltage is regulated by directly controlling the phase-shift angle, ϕ, between the two converter bridges. A simple proportional-integral (PI) controller is used to effect a change in the control variable, ϕ. The model, given in (3) and (4), is used to extract the plant transfer function.

TABLE I: System parameters

Parameter	Variable	Value
Input DC voltage	v_{in}	500 V
Output DC voltage	v_c	270 V
Switching frequency	f_s	50 kHz
Transformer turns-ratio	n	0.41
Power transfer inductance	L	9.8 μH
Output capacitance	C	45 μF

The Bode diagram of the control-to-output transfer function is plotted in Fig. 4b. It indicates a single pole at 153 Hz, which corresponds to the time-constant related to the output filter capacitor and the load resistance. A proportional-integral (PI) controller is, typically, used to regulate the output voltage. The integral part of the PI controller removes the steady state error. Since, there is a pole available at 153 Hz, the zero of the PI controller is placed at this frequency to preserve the 20 dB/decade roll-off of the magnitude. A gain is introduced into the controller to achieve the required phase-margin of at least 74° and settling time of 1.6ms. The phase-margin is specified to obtain over-damped response, whereas the settling time is specified to allow for fair comparison with the *first harmonic current control* strategy introduced in the next section. The controller for the output voltage control is of the form given in (5).

$$G_{PI}(s) = K\left(1 + \frac{\omega_z}{s}\right) \quad \text{where,} \quad \omega_z = 2\pi f_z, \; K = 0.0021 \text{ rads/V}, f_z = 153 \text{ Hz} \tag{5}$$

IV. First Harmonic Current Control

In section II, the I-FHA model is shown to comprise of active power component of inductor current, $\Im\langle i_L \rangle_1$, as a state-variable. It is proposed to utilize this component of current to effect a change in the output voltage. The structure of the proposed control system is shown in Fig. 5a. A reference for the active component of current is generated through a controller acting upon the output voltage error. An inner current loop controller uses this reference to generate the control variable, ϕ. The feedback of the active component of current, for the inner loop, is computed in a DSP from the raw data captured by the current sensor. A method of computing this feedback is discussed in the later part of this section. The error signals for both voltage and current control loops in this strategy are multiplied by -1. It is because the active component of current is represented by $\Im\langle i_L \rangle_1$, which is aligned to the negative imaginary axis, as shown in Fig. 3b.

A. Design of inner loop control

The control (ϕ) to output ($\Im\langle i_L \rangle_1$) transfer function of the plant is shown using a Bode diagram in Fig. 5b. It shows a pole-zero pair close to each other, thereby approximately cancelling their effect. The objective is to design a proportional-integral (PI) controller, $G_{PI,i}(s)$, for the inner loop.

$$G_{PI,i}(s) = K\left(1 + \frac{\omega_z}{s}\right) \quad \text{where, } \omega_z = 2\pi f_z \tag{6}$$

It is important to note that the control loop is implemented in a digital signal processor (DSP) and executed once in every switching cycle (f_s); i.e. 50kHz. Hence, any pole-zero placement must be sufficiently lower than f_s, such that

$$\{f_p, f_z\} \leq 0.2 f_s \tag{7}$$

The zero of the PI controller is, therefore, placed at $0.2f_s$ or 10kHz. In the control-to-output transfer function, a double-pole resonance is appearing at the switching frequency. The controller, therefore, must attenuate the complimentary sensitivity function of the inner loop. The magnitude at the double-pole resonance is also dependent on the resistance present in series with the inductor, such as winding resistances in the magnetic elements and the on-state resistance of the semiconductor devices. It, in fact, helps in reducing the peak magnitude at the resonant double-pole. A suitable gain is, therefore, used to reduce it to under 0 dB. The parameters for the controller, described in (6), are given in Table II.

TABLE II: Controller parameters for inner loop control.

Parameter	Variable	Value
Gain	K	0.0008 rads/A
PI zero	f_z	10 kHz

The uncompensated and the compensated loop gain of the inner, current control loop is shown in Fig. 5c. It is clear that the phase-margin of the compensated system is sufficiently high.

B. Design of outer loop control

Generally, in PWM-VSC converter systems employing the two-loop control structure, the bandwidth of the outer, voltage control loop is at least 5 times lower than the inner, current control loop. This allows the designer to assume the closed-loop transfer function of the inner loop to be unity. However, if the outer loop has a bandwidth close to that of the inner loop, the closed-loop transfer function of the inner loop also appears as part of the plant transfer function, i.e.

$$G(s) = \left[\frac{G_{PI,i}(s) \cdot G_{\Im\langle i_L\rangle_1,\phi}(s)}{1 + G_{PI,i}(s) \cdot G_{\Im\langle i_L\rangle_1,\phi}(s)}\right] G_{v_c,\Im\langle i_L\rangle_1}(s) \tag{8}$$

The Bode diagram of the plant, as described in (8), is shown in Fig. 6a. The magnitude plot starts rolling off with a slope of 40dB/decade indicating presence of two poles near 500Hz. On the pole-zero map, it is observed that the two poles are at 686 Hz and 377 Hz.

First, a PI controller is designed to eliminate the steady-state error. The zero of the PI controller is placed at the geometric mean of the two poles (9), i.e. 509 Hz, so that the effect of the two poles is equally mitigated.

$$f_z = \sqrt{f_{p1} \cdot f_{p2}} \tag{9}$$

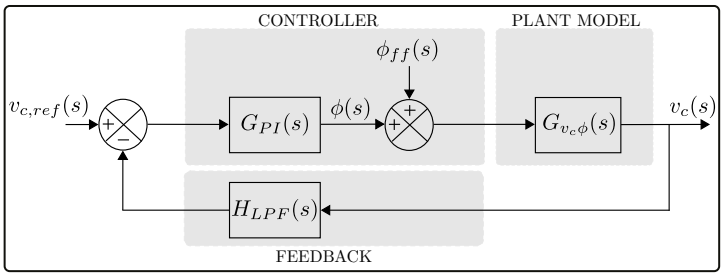

(a)

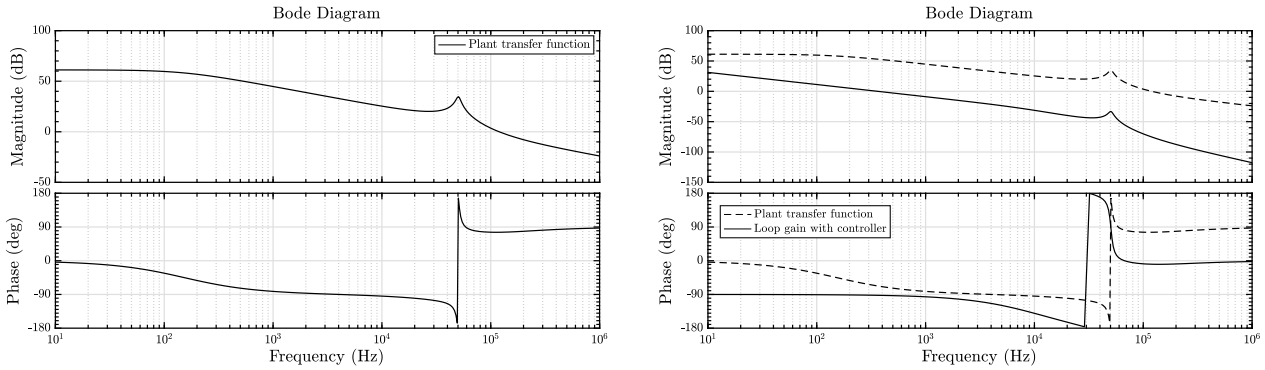

(b) (c)

Fig. 4: Output voltage controller: (a) Control schematic, and bode diagrams of (b) control-to-output transfer function, (c) uncompensated and compensated loop gain for control of output voltage through phase-shift angle, ϕ.

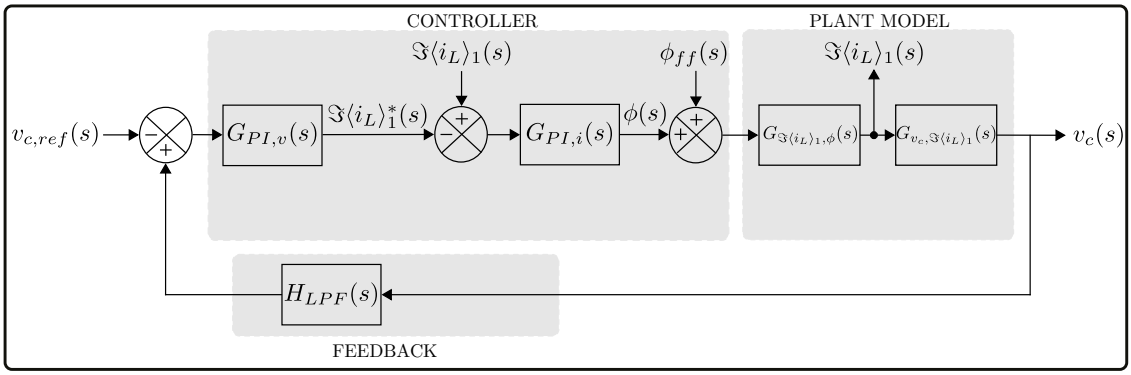

(a)

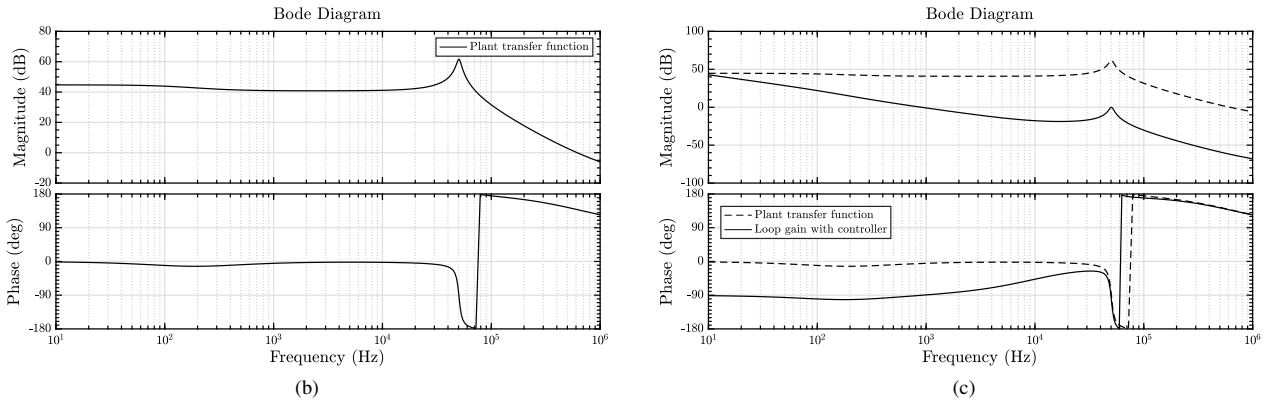

(b) (c)

Fig. 5: First harmonic current controller: (a) Control schematic, and bode diagrams of (b) control-to-output transfer function for inner, current control loop, (c) uncompensated and compensated loop gain for control of active power component of current.

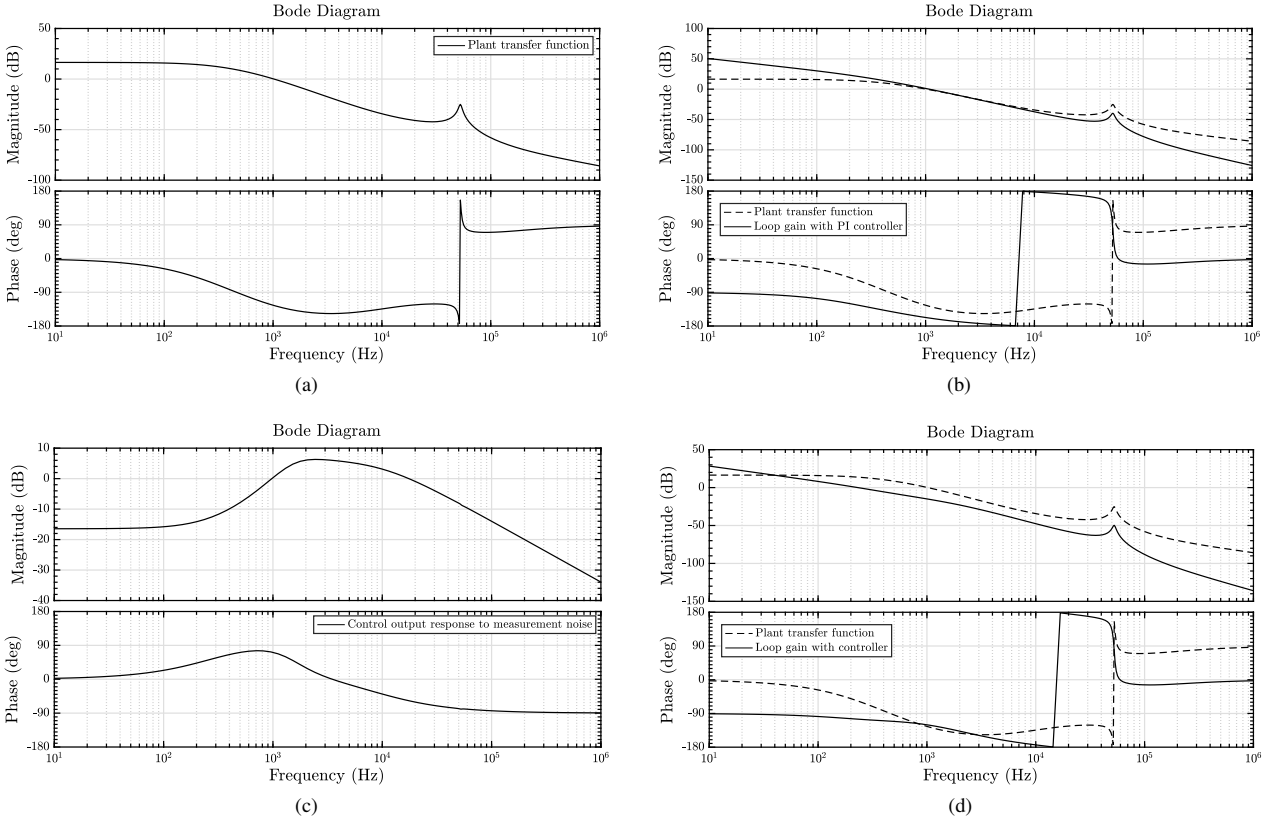

Fig. 6: Outer voltage loop controller design: Bode diagrams of (a) plant transfer function for outer voltage control loop, considering the closed loop transfer function of inner current loop, (b) plant transfer function and compensated loop gain with elementary PI control, (c) control output response to measurement noise with a PI controller followed by a unity gain lead compensator, and (d) plant transfer function and overall compensated loop gain.

The PI control, in conjunction with the poles of the plant, reduces the phase-margin to 21°. A lead compensator is, therefore, used to improve the phase-margin to 60° at a cross-over frequency of 1 kHz, as shown in Fig. 6b.

The pole and zero for the lead compensator, $f_{p,ld}$ and $f_{z,ld}$, can be calculated from the following equations.

$$\begin{aligned} f_m &= \sqrt{f_{p,ld} \cdot f_{z,ld}} \\ \sin\phi &= \frac{f_{p,ld} - f_{z,ld}}{f_{p,ld} + f_{z,ld}} \end{aligned} \tag{10}$$

Therefore, a lead compensator to increase the phase at f_m of 1000Hz by ϕ of 39° with an unity gain magnitude is given by:

$$\begin{aligned} G_{ld}(s) &= \sqrt{\frac{\omega_{z,ld}}{\omega_{p,ld}}} \frac{1 + s/\omega_{z,ld}}{1 + s/\omega_{p,ld}} \\ \text{where, } \omega_{p,ld} &= 2\pi f_{p,ld},\ \omega_{z,ld} = 2\pi f_{z,ld} \\ \text{and, } f_{p,ld} &= 2006 \text{ Hz},\ f_{z,ld} = 498 \text{ Hz} \end{aligned} \tag{11}$$

The control systems are, generally, designed using the compensated loop gain, sensitivity and complementary sensitivity functions. In Fig. 6c, the control output response to measurement noise is also examined. It shows a magnitude response exceeding unity at frequencies in the range of 1-10 kHz. It indicates that any measurement noise in the frequency range may result in amplified response at the controller output. If the attenuation due to the plant at this frequency is insufficient, it may result in unstable or oscillatory response. A suitable gain is, therefore, used to reduce the peak response of this transfer function to lower than -10dB.

The controller for the outer, voltage loop is given in (12) and the compensated loop gain response is shown in Fig. 6d.

$$\begin{aligned} G_{PI,v}(s) &= K\left(1 + \frac{\omega_z}{s}\right)\left(\frac{1 + \frac{s}{\omega_{z,\,ld}}}{1 + \frac{s}{\omega_{p,\,ld}}}\right) \\ \text{where, } \omega_z &= 2\pi f_z; \\ \omega_{z,ld} &= 2\pi f_{z,ld} \text{ and } \omega_{p,ld} = 2\pi f_{p,ld} \end{aligned} \tag{12}$$

TABLE III: Controller parameters for outer loop control.

Parameter	Variable	Value
Gain	K	0.0775 A/V
PI zero	f_z	509 Hz
Lead zero	$f_{z,ld}$	498 Hz
Lead pole	$f_{p,ld}$	2006 Hz

C. Implementation of inner loop control

The outer voltage control loop is implemented in a DSP in discrete domain using Tustin's transformation. The inner current loop, however, requires extraction of active power

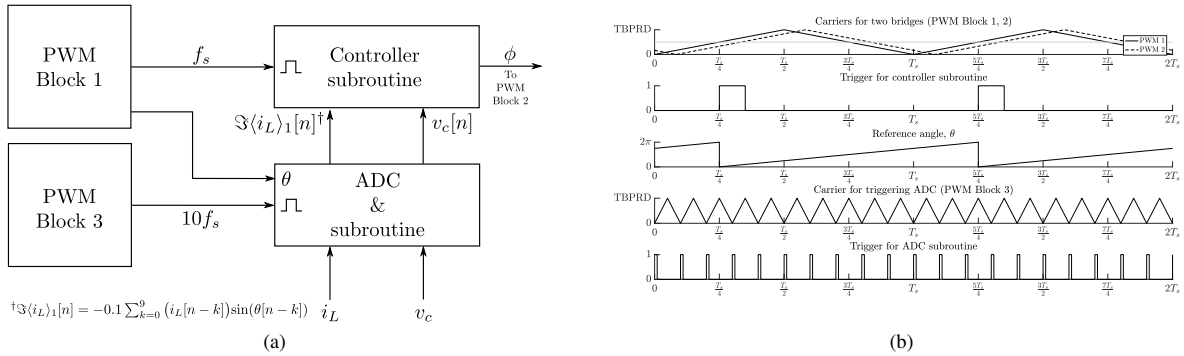

Fig. 7: Extraction of active power component of inductor current, $\Im\langle i_L\rangle_1$, in a DSP: (a) schematic for implementation in DSP, and (b) timing diagram for triggering ADC and control subroutines in the DSP.

component of current, $\Im\langle i_L\rangle_1$. Since, the inductor current is trapezoidal in nature, its fundamental component must be extracted and its position, referred to the AC voltage on primary-side bridge (Fig. 3b), must be known. The scheme is illustrated in Fig. 7a for implementation in a DSP. The timing diagram for triggering the analog-to-digital-converter (ADC) and the control algorithm is shown in Fig. 7b.

The reference angle, θ, is synchronized to the carrier wave of PWM block 1, which is locally generated in the DSP. The ADC is triggered 'n' times in one switching cycle. It is observed that $n = 10$ allows sufficient accuracy in the measurement of $\Im\langle i_L\rangle_1$. When the ADC is triggered, the product of instantaneous current, i_L, and sine of the reference angle, θ, is added to the sum of previous '$n-1$' values. This sum is then averaged over one switching cycle. The complete expression is given in (13). The negative sign in (13) indicates that the $\Im\langle i_L\rangle_1$ is aligned to the negative imaginary axis in the phasor diagram shown in Fig. 3b.

$$\Im\big\langle i_L\big\rangle_1[n] = -\frac{1}{n}\sum_{k=0}^{n-1}\Big((i_L[n-k])\sin(\theta[n-k])\Big) \qquad (13)$$

This value is the feedback signal, $\Im\langle i_L\rangle_1$, that is used with the current controller. The memory requirement for this computation is low, as the ADC is triggered at specific and known 'n' points for which the sine calculations can be stored. The computation power required by this operation will, however, rise with increasing switching frequency, thereby limiting its application to low-frequency, high-power converters.

V. Results and Discussion

In this section, the *output voltage control* and *first harmonic current control* strategies are validated through time-domain simulations and hardware experiments. A step-decrease of 30V in the output voltage reference is executed to validate the reference tracking ability of the developed control strategies. The experimental results, with the secondary side inductor current and the output voltage waveforms, for both strategies are reported in Fig. 8. A zoom-in for the current waveform, at the instant of step-change, is also presented to exhibit the transient DC appearing at this instant. In Fig. 9a, it is shown that there is good agreement in reference tracking results between the experiments, time-domain simulations and developed control models. The settling times of step-responses for both control strategies are, by design, approximately, 1.6ms. The step-responses obtained from simulations and experiments have been scaled to the same base as the model.

The *first harmonic current control* strategy is capable of controlling the active component of the current. Additionally, it is able to mitigate the transient DC appearing in the inductor current when a step-change in reference is executed, in comparison to that observed in *output voltage control*. It is demonstrated through time-domain simulations in Fig. 9b. In case of *output voltage control*, the peak magnitude of the transient DC observed in the inductor current is approximately 5A; in comparison, it is approximately 1.3A in case of *first harmonic current control*. The result indicates that a smaller safety margin in the peak flux density of the inductor and peak semiconductor current may be sufficient when *first harmonic current control* strategy is employed.

VI. Conclusions

The paper proposes a current control strategy which regulates output voltage through direct control of active power component of inductor current in a dual active bridge converter. The design and implementation of two control strategies: conventional *output voltage control* and the proposed *first harmonic current control* are presented. A complete design methodology for the two strategies has been suggested. A method to extract the active power component of current has been proposed and implemented; it is, however, limited to low-frequency, high-power converter applications. Experimental results at rated application voltage and power are reported and compared for the two strategies. The time-domain simulations and experimental results are in good agreement with the developed models of both the control strategies. The ability of the *first harmonic current control* to regulate the output voltage through control of active power component of current is demonstrated. Further, it is also shown to mitigate the transient DC in the inductor current when a step-change in reference is applied; it reduces the peak flux density of the power transfer inductor and peak semiconductor current. The control method can be developed further to decouple the active and circulating powers in a DAB converter, which may allow fulfilment of multiple control objectives.

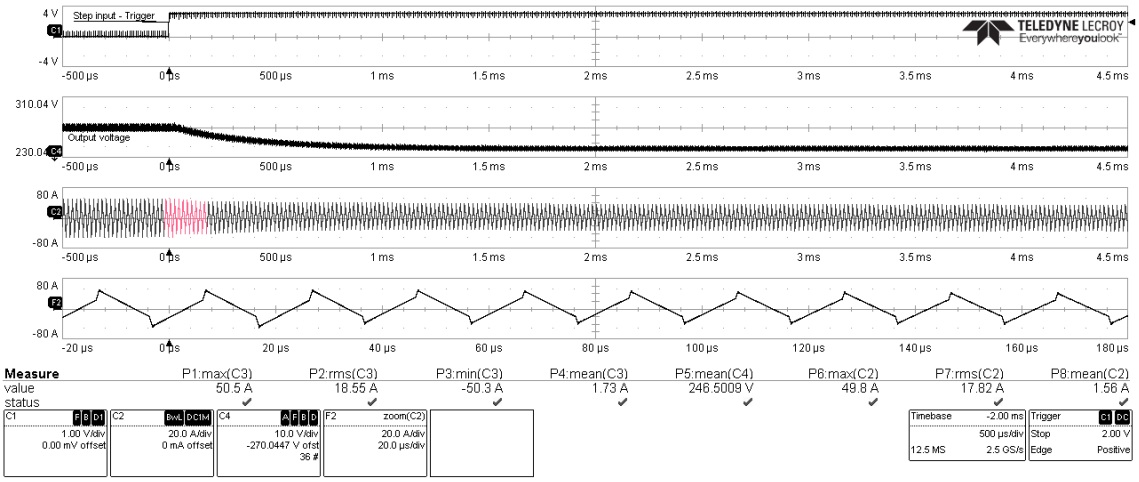

(a)

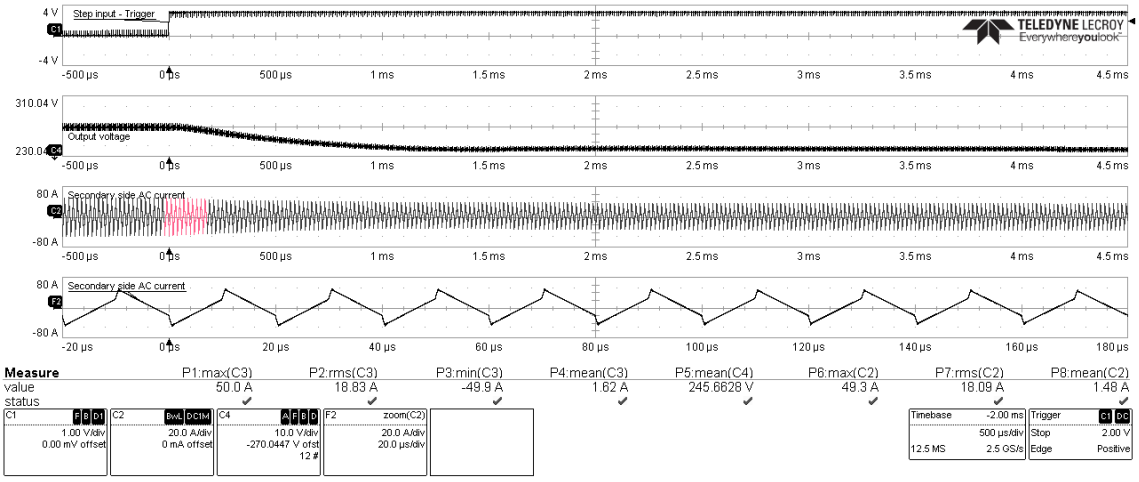

(b)

Fig. 8: Experimental results – response to a 30V step-decrease in output voltage reference: (a) *output voltage control*, and (b) *first harmonic current control*.

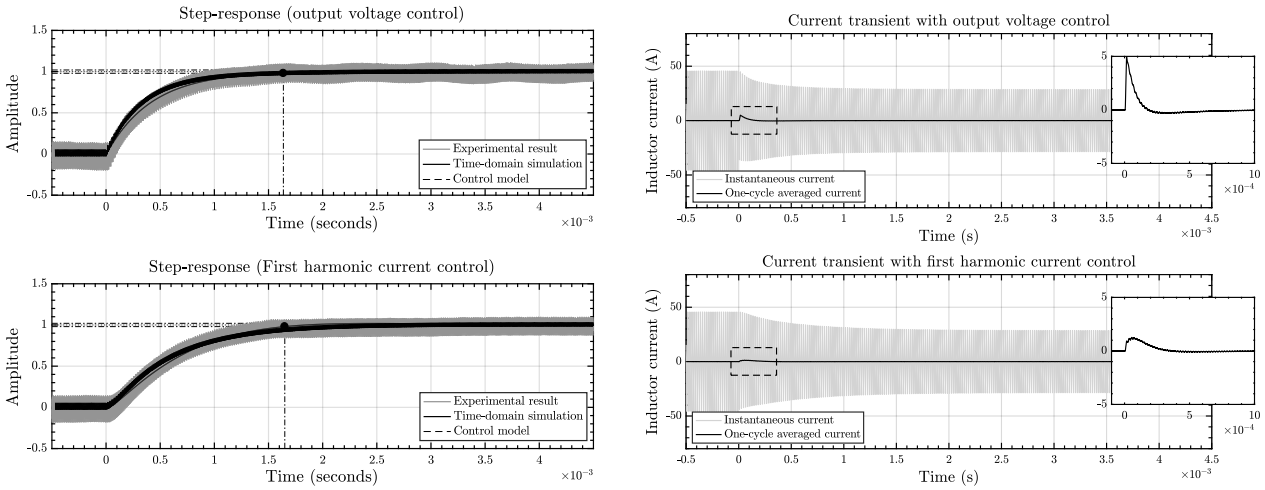

(a) (b)

Fig. 9: Response to step-change in output voltage reference: (a) comparison between experiments, time-domain simulations and control models - the settling time is marked, and (b) comparison of transient DC in the inductor current in time-domain simulations.

REFERENCES

[1] R. W. A. A. D. Doncker, D. M. Divan, and M. H. Kheraluwala, "A three-phase soft-switched high-power-density DC/DC converter for high-power applications," *IEEE Transactions on Industry Applications*, vol. 27, no. 1, pp. 63–73, Jan. 1991.

[2] T. Zhao, J. Zeng, S. Bhattacharya, M. E. Baran, and A. Q. Huang, "An average model of solid state transformer for dynamic system simulation," in *2009 IEEE Power Energy Society General Meeting*, Jul. 2009, pp. 1–8.

[3] J. Walter and R. W. D. Doncker, "High-power galvanically isolated DC/DC converter topology for future automobiles," in *Power Electronics Specialist Conference, 2003. PESC '03. 2003 IEEE 34th Annual*, vol. 1, Jun. 2003, pp. 27–32 vol.1.

[4] S. S. Shah and S. Bhattacharya, "Large & small signal modeling of dual active bridge converter using improved first harmonic approximation," in *2017 IEEE Applied Power Electronics Conference and Exposition (APEC)*, Mar. 2017, pp. 1175–1182.

[5] N. Soltau, H. A. B. Siddique, and R. W. D. Doncker, "Comprehensive modeling and control strategies for a three-phase dual-active bridge," in *2012 International Conference on Renewable Energy Research and Applications (ICRERA)*, Nov. 2012, pp. 1–6.

[6] H. Qin and J. Kimball, "Generalized Average Modeling of Dual Active Bridge DC-DC Converter," *IEEE Transactions on Power Electronics*, vol. 27, no. 4, pp. 2078–2084, Apr. 2012.

[7] K. Zhang, Z. Shan, and J. Jatskevich, "Large- and Small-Signal Average Value Modeling of Dual-active-bridge DC-DC Converter Considering Power Losses," *IEEE Transactions on Power Electronics*, vol. PP, no. 99, pp. 1–1, 2016.

[8] S. Han, I. Munuswamy, and D. Divan, "Preventing transformer saturation in bi-directional dual active bridge buck-boost DC/DC converters," in *2010 IEEE Energy Conversion Congress and Exposition (ECCE)*, Sep. 2010, pp. 1450–1457.

[9] J. Huang, Y. Wang, Z. Li, and W. Lei, "Predictive valley-peak current control of isolated bidirectional dual active bridge DC-DC converter," in *2015 IEEE Energy Conversion Congress and Exposition (ECCE)*, Sep. 2015, pp. 1467–1472.

[10] S. Dutta, S. Hazra, and S. Bhattacharya, "A Digital Predictive Current-Mode Controller for a Single-Phase High-Frequency Transformer-Isolated Dual-Active Bridge DC-to-DC Converter," *IEEE Transactions on Industrial Electronics*, vol. 63, no. 9, pp. 5943–5952, Sep. 2016.

[11] G. Kunov, I. Iatcheva, D. Marinov, E. Gadjeva, and I. Yatchev, "Bidirectional DAB DC-DC converter with hysteresis current mode control," in *2016 IEEE International Power Electronics and Motion Control Conference (PEMC)*, Sep. 2016, pp. 69–74.

[12] K. Takagi and H. Fujita, "Dynamic control and performance of an isolated dual-active-bridge DC-DC converter," in *2015 9th International Conference on Power Electronics and ECCE Asia (ICPE-ECCE Asia)*, Jun. 2015, pp. 1521–1527.

[13] B. Zhao, Q. Song, W. Liu, and Y. Zhao, "Transient DC Bias and Current Impact Effects of High-Frequency-Isolated Bidirectional DC-DC Converter in Practice," *IEEE Transactions on Power Electronics*, vol. 31, no. 4, pp. 3203–3216, Apr. 2016.

[14] X. Li and Y. F. Li, "An Optimized Phase-Shift Modulation For Fast Transient Response in a Dual-Active-Bridge Converter," *IEEE Transactions on Power Electronics*, vol. 29, no. 6, pp. 2661–2665, Jun. 2014.

[15] B. P. Baddipadiga and M. Ferdowsi, "Dual loop control for eliminating DC-bias in a DC-DC dual active bridge converter," in *2014 International Conference on Renewable Energy Research and Application (ICRERA)*, Oct. 2014, pp. 490–495.

[16] Y. Panov, M. M. Jovanovi, and B. T. Irving, "Novel transformer-flux-balancing control of dual-active-bridge bidirectional converters," in *2015 IEEE Applied Power Electronics Conference and Exposition (APEC)*, Mar. 2015, pp. 42–49.

[17] G. Ortiz, L. Fssler, J. W. Kolar, and O. Apeldoorn, "Flux Balancing of Isolation Transformers and Application of 'The Magnetic Ear'; for Closed-Loop Volt-Second Compensation," *IEEE Transactions on Power Electronics*, vol. 29, no. 8, pp. 4078–4090, Aug. 2014.

[18] S. R. Sanders, J. M. Noworolski, X. Z. Liu, and G. C. Verghese, "Generalized averaging method for power conversion circuits," in , *21st Annual IEEE Power Electronics Specialists Conference, 1990. PESC '90 Record*, 1990, pp. 333–340.